

Modeling for  
Wind Farm Control

A THESIS  
SUBMITTED TO THE FACULTY OF THE GRADUATE SCHOOL  
OF THE UNIVERSITY OF MINNESOTA  
BY

Jennifer Annoni

IN PARTIAL FULFILLMENT OF THE REQUIREMENTS  
FOR THE DEGREE OF  
MASTER OF SCIENCE

Peter Seiler, Advisor

May 2014

© Jennifer Annoni 2014

# Abstract

Wind turbines are typically operated to maximize their own performance without considering the impact of wake effects on nearby turbines. There is the potential to increase total power and reduce structural loads by properly coordinating the individual turbines in a wind farm. The effective design and analysis of such coordinated controllers requires turbine wake models of sufficient accuracy but low computational complexity. First, we formulate a coordinated control problem for a two-turbine array. Next, we review several simulation tools that range from low-fidelity, quasi-static models to high-fidelity, computational fluid dynamic models. These tools are compared by evaluating the power, loads, and flow characteristics for the coordinated two-turbine array. The results highlight the advantages and disadvantages of existing wake models for design and analysis of coordinated wind farm controllers. Finally, a dynamic medium fidelity wake model is constructed and compared to experimental results obtained from LiDAR wake measurements of the Clipper Turbine in UMore Park, Rosemount, MN.

# Contents

<b>List of Figures</b>	<b>iv</b>
<b>Chapter 1 Introduction</b>	<b>1</b>
<b>Chapter 2 Background</b>	<b>4</b>
2.1 Single Turbine Operation . . . . .	4
2.2 The Lanchester-Betz-Joukowsky Limit: Single Turbine Performance .	8
2.3 Wake Characteristics . . . . .	8
2.3.1 Turbine Modeling . . . . .	9
2.4 Two-Turbine Modelling . . . . .	10
2.4.1 Axial Induction Control . . . . .	10
<b>Chapter 3 Wake Model Implementation</b>	<b>13</b>
3.1 Park Model . . . . .	13
3.2 Dynamic Wake Meandering Model . . . . .	14
3.3 Actuator Disk Model . . . . .	16
3.4 Simulator for On/Offshore Wind Farm Applications . . . . .	20
<b>Chapter 4 Comparing Wake Models</b>	<b>22</b>

4.1	Simulation and Comparison of Wake Models . . . . .	22
4.2	Open Loop Coordinated Control . . . . .	24
4.3	Summary of Control Design and Analysis . . . . .	26
<b>Chapter 5</b>	<b>Model Validation</b>	<b>29</b>
5.1	Experimental Setup . . . . .	29
5.2	Results . . . . .	31
<b>Chapter 6</b>	<b>Conclusion</b>	<b>35</b>
	<b>Bibliography</b>	<b>37</b>

# List of Figures

2.1	$C_p$ Curve of the 2.5MW Clipper Turbine at UMore Park, Minnesota . . . . .	5
2.2	Regions of Wind Turbine Operation. . . . .	5
2.3	Block Diagram of a Standard Generator Torque Controller. . . . .	7
2.4	Block Diagram of a Standard Blade Pitch Controller. . . . .	7
2.5	Streamtube Control Volume of a Turbine. . . . .	8
2.6	Definition of Near and Far Wake of a Single Turbine. . . . .	9
2.7	Two Turbine Setup for Coordinated Control. . . . .	11
3.1	Setup for Deriving the Park Model. . . . .	13
3.2	Linear Forces defined on the turbine represented by an actuator disk. . . . .	17
3.3	Prandtl Mixing Length Theory. . . . .	18
3.4	Streamwise and spanwise velocity components of the actuator disk model . . . . .	19
3.5	One turbine (left) and two turbine (right) simulations with SOWFA . . . . .	20
4.1	Comparison of Streamwise Velocity Downstream of the Turbine. . . . .	23
4.2	Power, Power Variance, and Tower Loads Computed for each model. . . . .	24
4.3	Percent Increase predicted using axial induction control. . . . .	25
4.4	Streamwise Velocity of Park Model vs. Actuator Disk. . . . .	27

5.1	Clipper Wind Turbine located in UMore Park, Rosemount, MN (left). LIDAR used to measure wake profiles at various distances downstream (right) . . . . .	30
5.2	Wind Turbine/LIDAR Experimental Setup. . . . .	30
5.3	Wake Profiles gathered by LIDAR. . . . .	32
5.4	Actuator Disk with Comparisons of Downstream LIDAR Measurements. . . . .	33
5.5	Operating Conditions during Experiments. . . . .	33

# Chapter 1

## Introduction

Many states in the United States have set renewable portfolio standards that mandate renewable energy targets. For example, Minnesota has a target of 25% renewable energy by 2025 [1]. Wind energy is a fast growing source of renewable energy, therefore it is a key component to meet these standards. Achieving these targets requires increasing the efficiency and reducing the overall costs of wind energy. In particular, increasing the power capture efficiency of existing wind farms is critical as suitable land for turbines is decreasing. In addition, reducing structural loads on turbines will improve the economic competitiveness of wind energy by reducing the operation and maintenance costs.

Normally, wind turbines are controlled individually to maximize their own performance. Many studies have shown that operating all turbines in a wind farm at their optimal operating point leads to suboptimal performance of the overall wind farm [2], [3], [4], [5], [6], [7], [8]. An improved understanding of the aerodynamic interactions between turbines can aid in the design of enhanced control strategies that coordinate all turbines in a farm. The papers cited above present coordinated turbine control strategies with the aim of increasing the total wind farm power and, in some cases, reducing the structural loads. Essentially, the idea is that derating the lead turbine results in higher wind speeds for downstream turbines. Proper derating can result in a higher total power than simply operating each turbine at its own peak efficiency.

Most prior work on coordinated turbine control has used simplified actuator disk models for the design and analysis. More accurate wake modeling is necessary to help understand and quantify the aerodynamic interactions in a wind farm. A variety of wake models exist in literature that are useful for studying wind farm control. The simplest models are the Park model [9] and the eddy viscosity model [10]. These models provide a quick, preliminary description of the wake interactions in a wind farm. Also, there are various medium-fidelity tools, including the Dynamic Wake Meandering (DWM) model [11] and variations of the actuator disk model [12], [13], [14]. These medium-fidelity models give a more detailed description of the wake at a low computational cost. Finally, several high-fidelity computational fluid dynamics (CFD) models have been developed, e.g., [15], [16]. These high-fidelity models are the most accurate tools and can be used for evaluating wind farm controllers. However, they are computationally expensive.

Once these wake models are developed, there are limited resources in model validation. The University of Minnesota has a 2.5MW Clipper Turbine located in UMore Park, Rosemount, MN. Using a WINDCUBETM LiDAR, we can take measurements in the wake at various downstream distances, under varying wind conditions, and compare the results with these wake models.

This thesis investigates several wake models of varying fidelity and addresses their potential for control designs and analysis for optimal wind farm performance. To highlight the features of the various wake models, the focus is restricted to the coordination of a two-turbine array aligned with the wind. As a result, yaw misalignment and the superposition of multiple wakes are not considered in this thesis. See [17] for details regarding these topics. The first section formulates the coordinated control problem for the two-turbine array, which includes a description of single turbine control, a discussion on the theoretical maximum performance of wind turbines, and wake characteristics. The next section provides detailed descriptions for each wake model considered in this thesis. This thesis is not intended to compare all existing wake models. Instead, candidate models are selected for comparison based on the rough categorization of low, medium, and high fidelity. In addition, the models investigated here are available to the public. This thesis provides simulation results, and comparisons using the selected wake models. The results highlight the advantages and

disadvantages of each model. The final section of this thesis addresses preliminary model validation done using the Clipper turbine, specifically comparing experimental results to medium fidelity wake models. Conclusions and suggestions for future work are given at the end.

# Chapter 2

## Background

### 2.1 Single Turbine Operation

This section reviews the operation and control of a single turbine. Additional details and references can be found in [18], [19], [20]. Utility-scale turbines have several inputs that can be controlled to increase the captured power and reduce structural loads. These inputs include generator torque,  $\tau_g$ , and blade pitch,  $\beta$ , at varying wind speeds,  $u$ , which can control the rotor speed of the turbine,  $\omega$ . In general, the generator torque is varied at low wind speeds to maximize power captured. At high wind speeds, the blade pitch angle is used to mitigate mechanical and electrical loads. The power captured by a single turbine can be expressed by:

$$P = \frac{1}{2}\rho Au^3 C_P(\beta, \lambda) \quad (2.1)$$

where  $\rho$  [kg/m<sup>3</sup>] is the air density,  $A$  [m<sup>2</sup>] is the area swept by the rotor,  $u$  [m/s] is the wind speed perpendicular to the rotor plane, and  $C_P$  [unitless] is the power coefficient. The power coefficient is the fraction of available power in the wind captured by the wind turbine.  $C_P$  is a function of blade pitch angle,  $\beta$  [rad] and nondimensional tip-speed-ratio (TSR). Figure 2.1 is the normalized  $C_P$  curve of the 2.5 MW Clipper Turbine located in UMore Park. The peak efficiency has been normalized for proprietary reasons.

The standard turbine controller, with torque and blade pitch as inputs, can be split into 3 regions: Region 1, Region 2, and Region 3, see Figure 2.2. In Region 1,

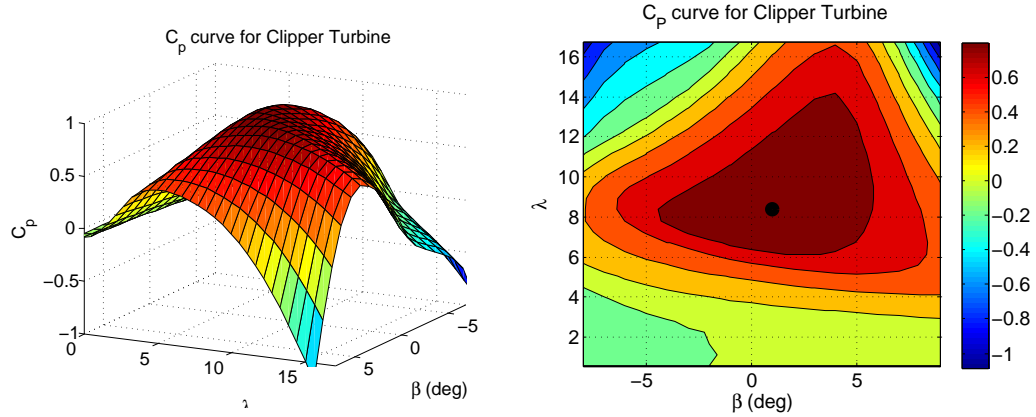


Figure 2.1:  $C_p$  Curve of the 2.5MW Clipper Turbine at UMore Park, Minnesota

the turbine does not produce any power because the wind speed is not sufficient to operate. Once the wind reaches the cut-in speed, the turbine enters Region 2. In this region, the turbine keeps the blades fixed at an optimal blade pitch angle and maximizes the generator torque to maximize the power of the turbine. Lastly, when the wind reaches the rated wind speed, the turbine is producing the maximum power that it is allowed to produce. In this region, the power is held constant by fixing the generator torque. The blades are pitched to minimize structural loads and maintain a constant rotor speed. The specifics of the controller operations in each region are addressed below.

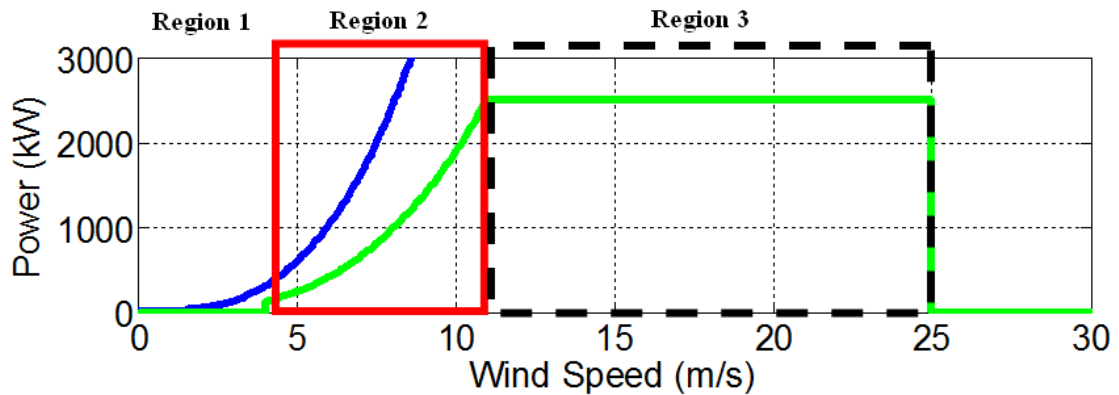


Figure 2.2: Regions of Wind Turbine Operation.

In Region 2, the controller typically used is a generator torque controller. The dynamics of the turbine are modeled as a single degree-of-freedom rotational system:

$$\dot{\omega} = \frac{1}{J} (\tau_{aero} - \tau_g) \quad (2.2)$$

where  $\dot{\omega}$  [ $rad/s^2$ ] is the angular acceleration,  $\tau_{aero}$  [Nm] is the aerodynamic torque, and  $\tau_g$  [Nm] is the generator torque. The power captured by a turbine can be expressed in terms of rotor speed by:

$$P = \tau_{aero}\omega \quad (2.3)$$

Using this relationship, the aerodynamic torque can be rewritten as:

$$\tau_{aero} = \frac{P}{\omega} = \frac{\rho A u^3 C_P(\beta, \lambda)}{2\omega} \quad (2.4)$$

The objective of a generator torque controller is to maximize power. This is done by maintaining an optimal blade pitch angle,  $\beta_*$  and TSR,  $\lambda_*$ . The blade pitch angle is held fixed at  $\beta_*$ , and the generator torque is controlled to achieve  $\lambda_*$  in varying wind conditions, Figure 2.3. The generator torque can be computed using the standard control law:

$$\tau_g = K_g \omega^2 \quad (2.5)$$

where  $K_g = \frac{C_{P_*} \rho A R^5}{2\lambda_*^3 N}$  and N is the gearbox ratio. If  $K_g$  is chosen properly, the power from the turbine will converge to  $C_{P_*}$  in steady winds. In turbulent winds, the turbine will cycle around the peak  $\lambda_*$ . Substituting  $\tau_{aero}$  and  $\tau_g$  into the single degree-of-freedom rotational system, it can be shown that the turbine will converge to toward the desired operating point  $C_{P_*}(\beta_*, \lambda_*)$

In Region 3, the turbine controller holds the generator torque constant and pitches the blades to keep the rotor speed constant at its rated speed and minimize structural loads.

It is common to use a proportional-integral or proportional-integral-derivative controller for blade pitch control [18], [19]:

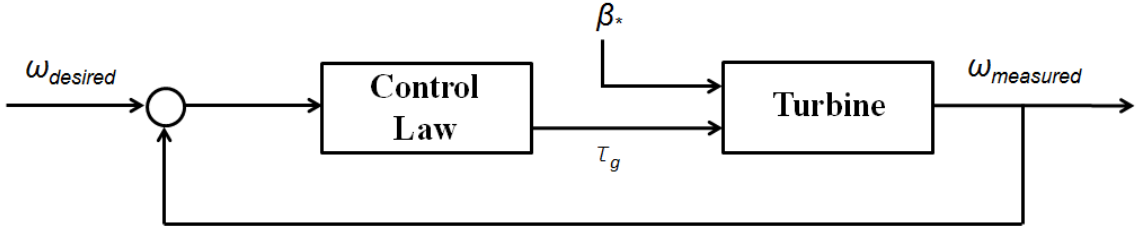


Figure 2.3: Block Diagram of a Standard Generator Torque Controller.

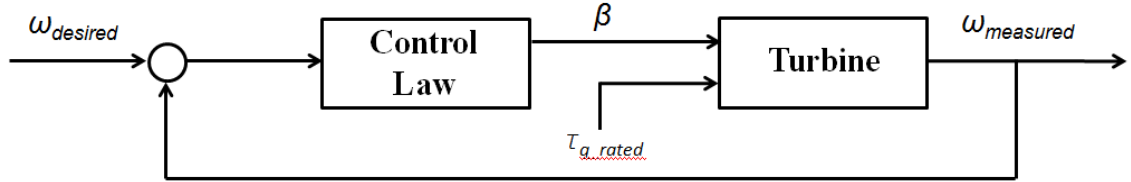


Figure 2.4: Block Diagram of a Standard Blade Pitch Controller.

$$\beta(t) = K_P e(t) + K_i \int_0^t e(\tau) d\tau + K_d \dot{e}(t) \quad (2.6)$$

$$e(t) = \omega_{rated}(t) - \omega(t) \quad (2.7)$$

where  $K_p$ ,  $K_i$ , and  $K_d$  are constants that can be chosen based on the desired performance of the turbine in this region.  $e$  is the difference between the rated rotor speed,  $\omega_{rated}$ , and the actual rotor speed. The blade pitch controller computes a blade pitch that will try to minimize  $e$ .

The performance of a single turbine can be simulated using the FAST model developed by the National Renewable Energy Laboratory (NREL) [21]. FAST is a nonlinear simulation package that models the dominant structural modes for a wind turbine, e.g., tower and blade bending modes. In addition, the aerodynamics forces on the blade are modeled using blade element theory. FAST can determine the power production and loading characteristics experienced by a single turbine for a given wind profile. However, it does not include the capability to model the effect of the turbine on the airflow including downstream wakes.

## 2.2 The Lanchester-Betz-Joukowski Limit: Single Turbine Performance

The maximum theoretical performance of a single turbine had been derived separately by Fredrick Lanchester, Albert Betz, and Nikolai Joukowsky in the early 1900s using an idealized actuator disk, i.e. independent of turbine design [22]. Consider a streamtube with an initial velocity,  $u_1$ , and a velocity behind the turbine,  $u_2$  (Figure 2.5). The turbine is represented by an actuator disk, S. If a turbine extracted 100% of the power out of the wind, the velocity behind the turbine would be 0 m/s, effectively blocking any wind from flowing through the turbine. Therefore, the velocity behind the turbine has to be nonzero for wind to flow through, but less than the initial velocity. The streamtube expands due to conservation of mass.

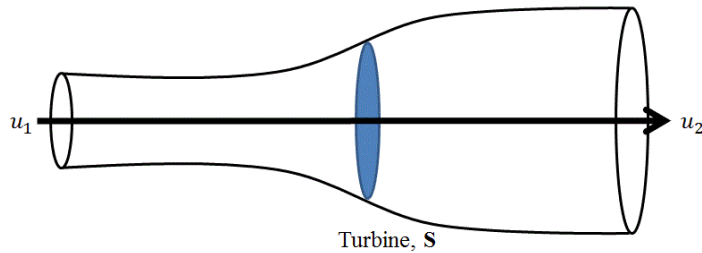


Figure 2.5: Streamtube Control Volume of a Turbine.

Using conservation of mass and momentum, it has been shown that the maximum power coefficient that a turbine can achieve is 0.593 or 59.3% of the power in the wind can be extracted by the turbine. See [20] for full derivation. In practice, utility scale turbines usually have a power coefficient around 0.4 to 0.5.

## 2.3 Wake Characteristics

The wind turbine operation creates a trailing wake that can be divided into two regions: the near wake and the far wake (Figure 2.6). The near wake is defined as the region that is 1 to 5 diameters downstream of the turbine where characteristics of the flow field are determined by the turbine geometry. The flow is driven by a strong nonzero pressure gradient and strong turbulence caused by tip vortices and separation of the flow at the blade edges. In addition, there is a strong acceleration around the

nacelle of the turbine that produces a velocity profile with a faster velocity in the center of the wake. The tip vortices break down at about 4 diameters downstream, making the transition from the near wake to the far wake.

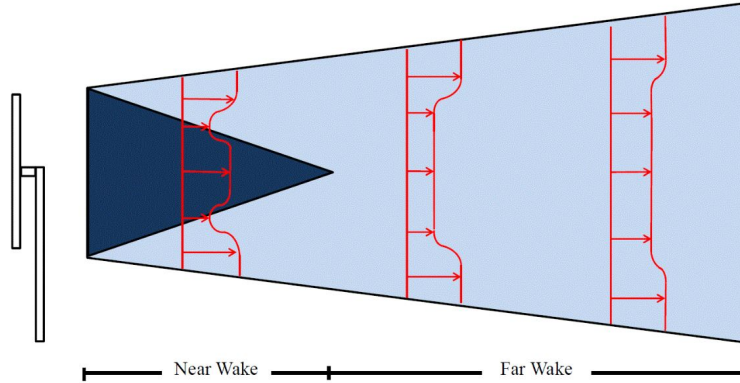


Figure 2.6: Definition of Near and Far Wake of a Single Turbine.

In the far wake, the pressure gradient becomes less significant, and the wake is less dependent on the turbine geometry and more on topographic effects. In this region, the tip vortices breakdown due to viscosity and induce mixing, which enhances the viscous effects. This mixing entrains fluid from outside the wake and causes the wake to recover to freestream velocity far downstream. As this wake recovers, it takes on a Gaussian-like profile. This region becomes approximately axisymmetric and self-similar, i.e., the wake at distances downstream take on a similar shape, making the wake easier to model [23]. This shape is independent of the geometry of the turbine. In this case, the thin boundary layer equations provide a useful approximation. The thin boundary layer equations are further addressed in the Wake Model Implementation section under the Dynamic Wake Meandering Model.

### 2.3.1 Turbine Modeling

A model of the turbine interaction with the flow field is required to simulate the downstream wake. As previously noted, the standard implementation of the FAST simulation package does not include such a model. Two alternative models are considered in this paper. Both of these models can interface with FAST. The first model is an actuator disk [23]. This is a porous disk that can be modeled having constant,

radial, or variable loading that influence the flow field. The advantage to using the actuator disk is that the blades of the turbine do not need to be modeled, which reduces the overall computation time.

The second more complex model is the actuator line [23]. This model takes finite sections of the rotating blade and calculates the airfoil lift and drag forces as they act on the flow. The lift and drag forces depend on the blade airfoil geometry and flow conditions. Nondimensional lift and drag are typically stored in a look-up table as a function of the angle of attack between airflow and blade chord. This model can take considerably more computing time. Both the actuator disk and actuator line models can be used in CFD wake models.

## 2.4 Two-Turbine Modelling

This section addresses axial induction control as a way to coordinate a two-turbine array. When looking at coordinated control of wind turbines, yaw control and wake superposition play an important role and have been addressed in the literature, but are not considered here. For additional information on yaw control, see [17]. For additional information on wake superposition, see [5].

### 2.4.1 Axial Induction Control

This section focuses on axial induction control for two-turbine array shown in Figure 2.7.

Let  $P_1$  and  $P_2$  denote the power from Turbines 1 and 2, respectively. As described previously, the power generated by the first turbine depends on the inflow wind speed as well as the blade pitch  $\beta_1$  and TSR,  $\lambda_1$ , for the turbine. The inflow speed for the first turbine is approximately equal to the free-stream velocity, i.e.,  $u = U_\infty$ , hence the power generated by Turbine 1 can be expressed as  $P_1(\beta_1, \lambda_1, U_{infty})$ . The operation of Turbine 1 disturbs the flow and this impacts the operation of the downstream turbine, i.e., Turbine 2. Specifically, the flow impacting the rotor on Turbine 2 depends on the blade pitch and TSR of Turbine 1. Thus the averaged power generated by Turbine 2 has a functional form of  $P_2(\beta_1, \lambda_1, \beta_2, \lambda_2, U_\infty)$ . The precise relationship describing the aerodynamic coupling between the turbines depends on the model used for the near/far wake. The total power generated by the two-turbine array is thus given by:

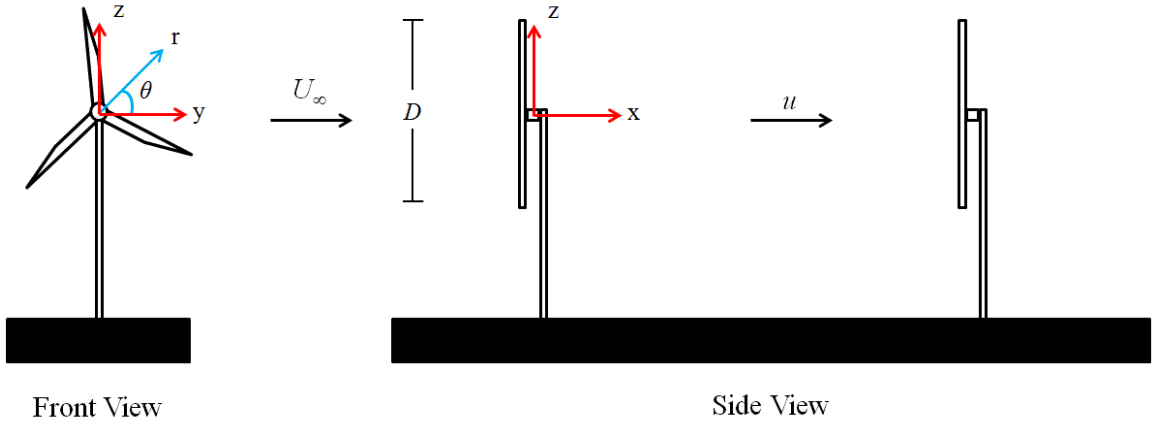


Figure 2.7: Two Turbine Setup for Coordinated Control.

$$P_{tot}(\beta, \lambda, U_{infty}) = P_1(\beta_1, \lambda_1, U_{infty}) + P_2(\beta, \lambda, U_{infty}) \quad (2.8)$$

where the vectors  $\beta := [\beta_1, \beta_2]^T$  and  $\lambda := [\lambda_1, \lambda_2]^T$  are defined to simplify the notation. The main objective of axial induction control is to maximize the total average power output:

$$\max_{\beta, \lambda} P_{tot}(\beta, \lambda, U_{infty}) \quad (2.9)$$

This problem formulation assumes a constant free-stream velocity  $U_{infty}$ , which is essentially a steady-state formulation. A low-level generator torque control law can be used to regulate the turbine to the optimal TSR. A more realistic formulation treats the free-stream velocity as unsteady and turbulent. In this case, the objective is to maximize the average power generated by the two-turbine array. Moreover, the unsteady flow causes significant structural loads on the tower and blades of both turbines. Thus the formulation can be extended to include constraints on the loads. Alternatively, additional terms can be included in the objective function to trade off the power capture and loads.

The power maximization problem is difficult to solve as it involves complicated models of the turbine operation and wake interactions. As a result, previous work on turbine coordination [2], [3], [4], [5] has focused on simplified models for the turbine operation.

In particular, the induction factor for a single turbine is defined as  $a := 1 - \frac{u_1}{U_{infty}}$ , where  $u_1$  denotes the average horizontal speed across the rotor plane. The induction factor is a measure of how much the wind slows down due to the action of the turbine. In addition, the turbine induction factor can be related to the power and the thrust coefficient by the actuator disk theory [20]:

$$C_P = 4a(1 - a)^2 \tag{2.10}$$

$$C_T = 4a(1 - a) \tag{2.11}$$

The thrust coefficient is the ratio of the axial thrust force (perpendicular to the rotor plane) and the dynamic force on the rotor. The induction factor thus controls the power and thrust coefficient of a turbine and hence impacts the velocity deficit. Decreasing the power coefficient of the upstream turbine increases the velocity seen at the downstream turbine. Again, the precise relationship between the downstream wake and the induction factor of Turbine 1,  $a_1$ , depends on the wake model. Thus the power generated by a two-turbine array can potentially be increased by proper choice of the induction factors  $a := [a_1, a_2]$ . The power maximization problem formulated for this simplified turbine (actuator disk) model is given by:

$$\max_a P_{tot}(a, U_{infty}) \tag{2.12}$$

The connections between the simplified and more realistic maximization problems are described further in later sections.

# Chapter 3

## Wake Model Implementation

### 3.1 Park Model

The simplest wake model considered is the Park model [9], [24]. This model has been widely used in wind farm control literature in recent years [2], [3], [5], [6]. The Park model has the lowest fidelity and requires the least computational time of the models addressed in this paper. The Park Model is setup up as in Figure 3.1. The turbine is modeled as an actuator disk with uniform axial loading in a steady uniform flow. The velocity is assumed to be constant in the wake at a given downstream distance and the wake increases linearly downstream. This model is only valid for the far wake.

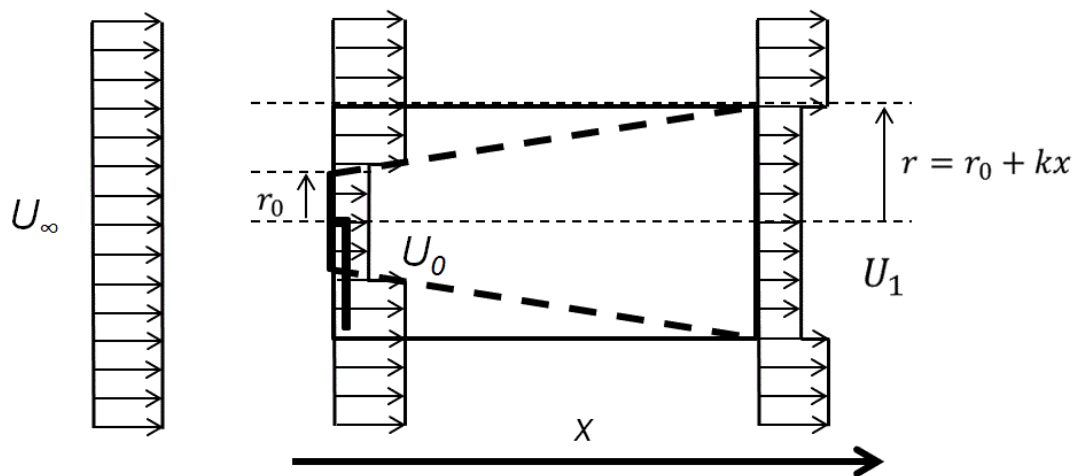


Figure 3.1: Setup for Deriving the Park Model.

Consider the example of a turbine operating in a freestream velocity  $U_\infty$  as shown in Figure 3.1. The diameter of the turbine rotor plane is denoted by  $D = 2r_0$  and the turbine is assumed to be operating at an induction factor  $a$ . A cylindrical coordinate system is placed at the rotor hub of the first turbine with the downstream and radial distances denoted by  $x$  and  $r$ , respectively. The velocity profile at a location  $(x, r)$  is:

$$u_1(x, r; a) = U_\infty(1 - \delta u(x, r; a)) \quad (3.1)$$

where the velocity deficit  $u$  is given by:

$$\delta u = \begin{cases} 2a\left(\frac{D}{D+2kx}\right)^2, & r \leq \frac{D+2kx}{2}. \\ 0, & \text{else} \end{cases} \quad (3.2)$$

In this model, the velocity,  $u$ , is defined in the axial ( $x$ ) direction and remaining velocity components are neglected. The wake is parameterized by a tuneable non-dimensional wake decay constant  $k$  [25], [26].

The Park model can be used to compute the power production and velocity deficit of a turbine array. A 10-minute simulation can run in seconds on a desktop computer. This is useful in determining operating conditions of a wind farm to maximize power. However, it has no notion of turbulence in the downstream wake and cannot determine the structural loads on the turbines. In addition, the assumptions are based on a steady inflow acting on an actuator disk with uniform axial loading. Despite its limitations, the Park model can provide some insight of turbine interaction that can be used to understand the results obtained from higher-fidelity models.

### 3.2 Dynamic Wake Meandering Model

The next model considered is the DWM model [11]. The University of Massachusetts and NREL developed an implementation of the DWM model that was originally created at the Technical University of Denmark [27]. It couples the FAST model for an individual turbine with models for the wake deficit, turbulence, and (stochastic) meandering. The foundation of the wake deficit model used in the DWM model is the eddy viscosity model [10]. The wake deficit model numerically solves a simplified Navier-Stokes equation based on the thin boundary-layer approximation. The simpli-

fied Navier-Stokes equations assume a zero pressure gradient that is only valid in the far wake. Let  $x$  and  $r$  denote the downstream and radial distance from the turbine rotor hub as shown in Figure 2.7. In this model, the velocity components,  $u$  and  $v$ , are defined in the axial ( $x$ ) and the radial ( $r$ ) directions. The velocity components  $u$  and  $v$  satisfy the following partial differential equation:

$$u \frac{\partial u}{\partial x} + v \frac{\partial u}{\partial r} = -\frac{1}{r} \frac{\partial(\overline{ru'v'})}{\partial r} \quad (3.3)$$

The right-hand side of this equation can further be described in terms of turbulent viscosity, :

$$-\overline{(u'v')} = \epsilon \frac{\partial u}{\partial r} \quad (3.4)$$

where  $u'$  and  $v'$  denote the fluctuating velocity components in the axial and radial directions and  $\overline{u'v'}$  is a temporal average that represents a turbulent momentum flux that acts like a stress, also known as a Reynolds stress. The turbulent viscosity,

$$\epsilon = k_2 b (u_\infty - u_c) \quad (3.5)$$

describes the shear stresses and eddy viscosity in the wake, where  $b$  is the wake half width,  $u_c$  is the center wake velocity, and  $k_2$  is an empirical constant of the flow field typically set to 0.009.

The DWM model uses Taylors hypothesis when modeling turbulence. This hypothesis assumes that the turbulence has no effect on the wake advection, i.e., wake transport, from upstream to downstream. A consequence of this hypothesis is that the wake advection is only a function of the mean wind speed. The DWM model is interfaced with a FAST turbine model as follows. The first turbine is simulated in FAST with a three-dimensional input wind field. The DWM model is then used to calculate the downstream wake based on the FAST simulation results for Turbine 1. The downstream wake is then linearly superimposed on the wind field to generate the velocity conditions for the downstream turbine, i.e., Turbine 2. Finally, a FAST simulation is performed for Turbine 2 using this wake superimposed wind profile.

The advantage of the DWM model over the Park model is that it gives a more realistic representation of the far wake at a low computational cost. The DWM model can be used to compute the power production, velocity deficit, and loads of a turbine array. The turbines are modeled as actuator disks coupled with FAST and can handle steady and unsteady inflows. In addition, the DWM model can run in minutes on a desktop computer. The disadvantage of the DWM model is that it is not suitable for feedback control design because it calculates the wakes of a wind turbine array one at a time, i.e., it does not provide a continuous flow. This complicates the use of this model for dynamic wind farm control.

### 3.3 Actuator Disk Model

The actuator disk model considered in this paper solves the 2D unsteady, Navier-Stokes equations by using the streamfunction ( $\psi$ ) vorticity ( $\omega$ ) formulation assuming the flow is incompressible. Similar implementations have been done in [12], [28]. Let  $(u, v)$  denote the streamwise and spanwise velocity components and  $(x, y)$  denote the downstream and spanwise distances. Vorticity can be defined as  $\omega = \frac{\partial v}{\partial x} - \frac{\partial u}{\partial y}$  and the streamfunction can be defined in terms of the streamwise and spanwise velocity components:  $\frac{\partial \psi}{\partial x} = -v$  and  $\frac{\partial \psi}{\partial y} = u$ . Under some additional technical assumptions, the Navier-Stokes equations are reformulated to the following governing equations using vorticity and streamfunction:

$$\frac{\partial \omega}{\partial t} + u \frac{\partial \omega}{\partial x} + v \frac{\partial \omega}{\partial y} = \nu \left( \frac{\partial^2 \omega}{\partial x^2} + \frac{\partial^2 \omega}{\partial y^2} \right) - \frac{1}{\rho} \frac{\partial f_x}{\partial y} \quad (3.6)$$

$$\frac{\partial^2 \psi}{\partial x^2} + \frac{\partial^2 \psi}{\partial y^2} = -\omega \quad (3.7)$$

where  $f_x$  is the volume force of the actuator disk on the flow in the axial direction. These equations are the transport of vorticity and the Poisson equation for the stream function. The velocity components  $(u, v)$  can be computed from  $(\psi, \omega)$ . The turbines are modeled as actuator disks with a specified volume force acting on the flow. The loading on the actuator disk in this model is defined linearly (Figure 3.2).

The force is smallest in the middle and largest at the tips of the blades because the tips of the blades have the greatest impact on the flow due to deflections. These equations are solved using standard CFD methods [29].

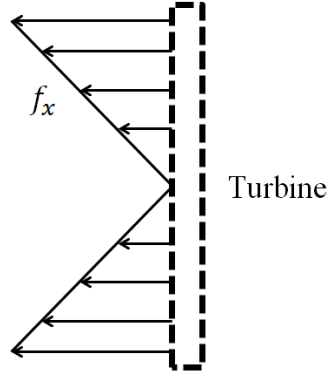


Figure 3.2: Linear Forces defined on the turbine represented by an actuator disk.

These equations are used to calculate the flow in a laminar region. However, the wake of the turbine is turbulent. To address this issue, Reynolds averaging is used to obtain the Reynolds Averaged Navier Stokes (RANS) equations:

$$\frac{\partial \langle U \rangle}{\partial x} + \frac{\partial \langle V \rangle}{\partial y} = 0 \quad (3.8)$$

$$\frac{\partial \langle U \rangle}{\partial t} + \langle U \rangle \frac{\partial \langle U \rangle}{\partial x} + \langle V \rangle \frac{\partial \langle U \rangle}{\partial y} = -\frac{1}{\rho} \frac{\partial \langle P \rangle}{\partial x} + \nu \left( \frac{\partial^2 \langle U \rangle}{\partial x^2} + \frac{\partial^2 \langle U \rangle}{\partial y^2} \right) + \frac{\partial \langle u'v' \rangle}{\partial y} + \frac{\langle u'^2 \rangle}{\partial x} \quad (3.9)$$

$$\frac{\partial \langle V \rangle}{\partial t} + \langle U \rangle \frac{\partial \langle V \rangle}{\partial x} + \langle V \rangle \frac{\partial \langle V \rangle}{\partial y} = -\frac{1}{\rho} \frac{\partial \langle P \rangle}{\partial y} + \nu \left( \frac{\partial^2 \langle V \rangle}{\partial x^2} + \frac{\partial^2 \langle V \rangle}{\partial y^2} \right) + \frac{\partial \langle u'v' \rangle}{\partial x} + \frac{\langle v'^2 \rangle}{\partial y} \quad (3.10)$$

The last two terms in the x-momentum and the y-momentum equations are called the Reynolds stresses, specifically  $\langle u'^2 \rangle$ ,  $\langle u'v' \rangle$ ,  $\langle v'^2 \rangle$ , and  $\langle v'u' \rangle$ , and are present in turbulent flows. These terms cause the diffusion of momentum normal to the flow direction and enhance the viscous effects in the flow. This mixing causes the wake to recover more quickly downstream of the turbine. There are various ways to model this stress. For simplicity, the mixing length hypothesis is used to model these Reynolds stresses.

Figure 3.3 depicts the basic idea of Prandtl's mixing length theory. This assumes

that lumps of fluid, or eddies, maintain their streamwise momentum while mixing momentum in the transverse direction.

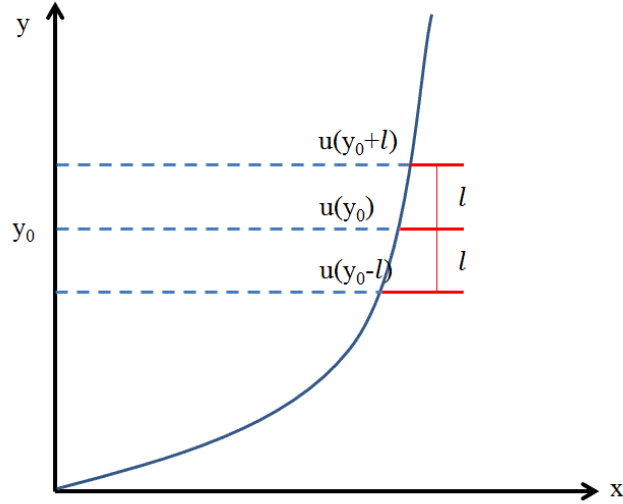


Figure 3.3: Prandtl Mixing Length Theory.

From Figure 3.3, the mixing length model can be derived by defining:

$$\Delta u_1 = u(y_0) - u(y_0 - l) = l \left( \frac{du}{dy} \right)_1 \quad (3.11)$$

$$\Delta u_2 = u(y_0 + l) - u(y_0) = l \left( \frac{du}{dy} \right)_1 \quad (3.12)$$

where  $l$  is the mixing length based on the geometry of the flow. For this case,  $l$  was taken to be a constant multiplied by the half-width of the wake. The half-width of the wake is defined based on free shear flow for axisymmetric wake assumptions found in [30]:

$$l = const. * x^{\frac{1}{2}} \quad (3.13)$$

The constant is determined based on simulated or experimental results. By taking the time average of the absolute value of  $\Delta u_1$  and  $\Delta u_2$ , the time-averaged fluctuations in the streamwise direction can be defined as:

$$|\bar{u}'| = \frac{1}{2} (|\Delta u_1| + |\Delta u_2|) = l \cdot \frac{du}{dy} \quad (3.14)$$

Consider an eddy travelling at  $u(y_0 - l)$  and an eddy travelling at  $u(y_0 + l)$ . The eddies will move apart with a velocity of  $2u'$  and the space between the eddies will be filled with entraining fluid giving rise to  $v'$ . This implies that  $v'$  will be on the same order as  $u'$ . In this way we can define the Reynolds stress terms as:

$$\langle u'v' \rangle = l^2 \left( \frac{du}{dy} \right)^2 \quad (3.15)$$

The 2D RANS velocity equations can also be rewritten in terms of vorticity in 2D:

$$\frac{\partial \langle \Omega \rangle}{\partial t} + \langle U \rangle \frac{\partial \langle \Omega \rangle}{\partial x} + \langle V \rangle \frac{\partial \langle \Omega \rangle}{\partial y} = \nu \left( \frac{\partial^2 \langle \Omega \rangle}{\partial x^2} + \frac{\partial^2 \langle \Omega \rangle}{\partial y^2} \right) + \frac{\partial \langle u' \omega' \rangle}{\partial x} + \frac{\partial \langle v' \omega' \rangle}{\partial y} \quad (3.16)$$

For simplicity, the last two terms in the above equation are dealt with in a similar way as the Reynolds stresses described previously in the RANS equation. It is assumed that the mixing length is the same for both vorticity and momentum. This may be expanded upon in the future to model these stresses in more realistic fashion. Figure 3.4 shows the resulting streamwise and spanwise velocity components from the actuator disk model.

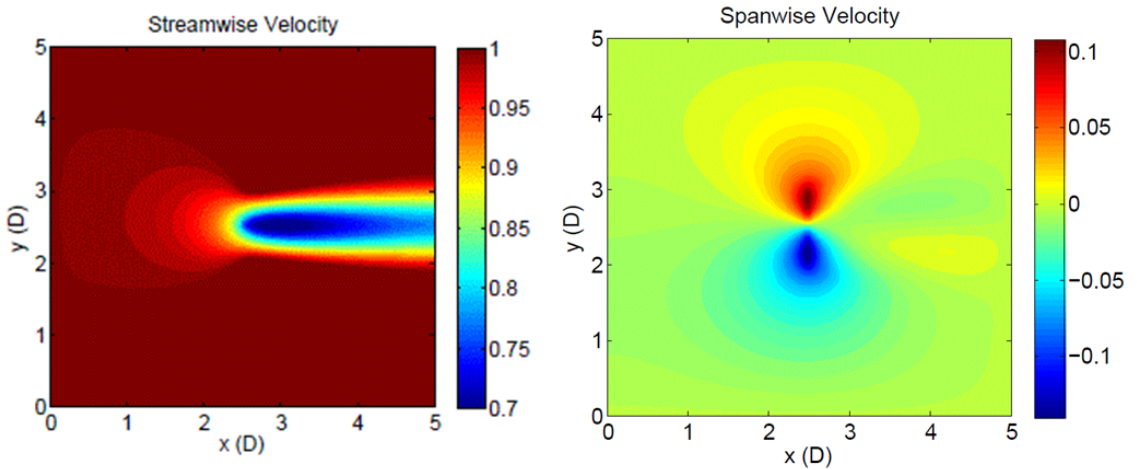


Figure 3.4: Streamwise and spanwise velocity components of the actuator disk model

This model uses an actuator disk to model the turbine. The near wake is dominated by tip vortices that are generated based on the blade geometry. The blades are not modeled in this simulation and as a result, this model cannot accurately depict the near wake region. However, this model captures the effects of the flow far downstream, greater than 3 diameters, where the flow is less dependent on turbine geometry. Therefore, this model is useful for studying the far wake of a turbine in steady and unsteady flows. The power production and velocity deficit of a turbine array can be computed within minutes on a desktop computer.

### 3.4 Simulator for On/Offshore Wind Farm Applications

SOWFA is a high-fidelity simulation tool that was developed at NREL to do offshore wind farm studies [16], [31], [32], [33], [34]. It can also be applied to land-based wind farms. SOWFA is a large-eddy simulation that is coupled with the FAST turbine model and based on the OpenFOAM open source toolbox.

SOWFA uses an actuator line model coupled with FAST to study turbines in the atmospheric boundary layer. SOWFA solves the three-dimensional incompressible Navier-Stokes equations and transport of potential temperature equations, which take into account the buoyancy and Coriolis effects. The buoyancy effect is caused by the temperature flux in the atmosphere and the Coriolis effect is the result of the rotation of the Earth.

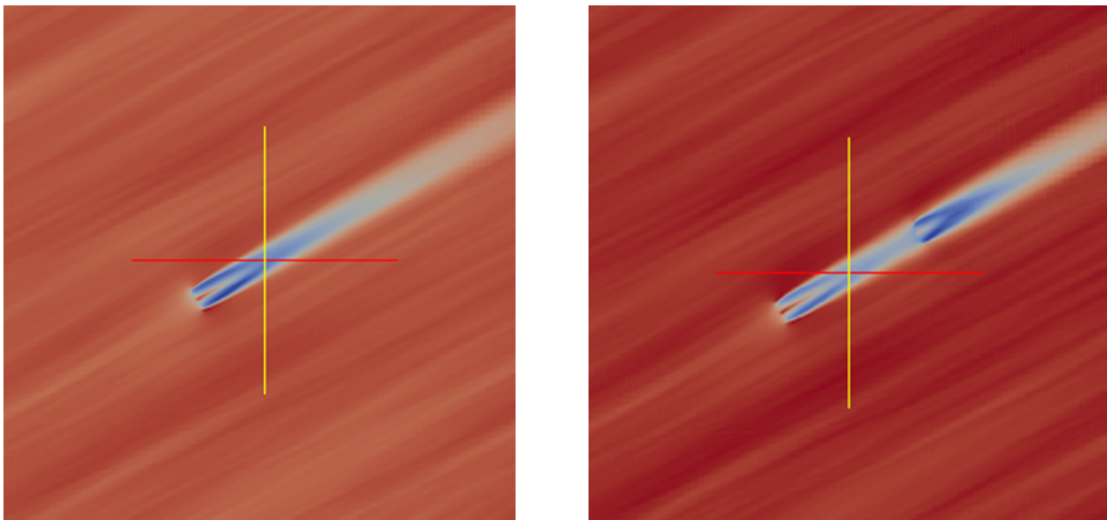


Figure 3.5: One turbine (left) and two turbine (right) simulations with SOWFA

SOWFA performs three-dimensional calculations that can describe the steady and unsteady flow field in the near and far wake. This information can be used to compute the power, velocity deficits, and loads at each turbine in a wind farm. This level of computation, with high-fidelity accuracy, takes on the order of days to run on a cluster using a few hundred processors [35], [36]. As a result, it would take considerable effort to perform feedback control design for a wind farm with this model. However, it is the highest fidelity model considered, hence its use is most suitable for evaluating wind farm controllers.

# Chapter 4

## Comparing Wake Models

### 4.1 Simulation and Comparison of Wake Models

The wake characteristics of each model were compared by simulating a two-turbine setup over 1000 s. The simulated turbines have a 126 m diameter and a hub height of 90 m. The wind speed has a mean of 8 m/s with 6% turbulence intensity.

Figure 4.1 compares the spatially-averaged streamwise velocity profile of a single turbine setup for each model. SOWFA is the highest fidelity model and has been validated against wind farm data [33], [34]. The Park and DWM model results match SOWFA in the far wake at distances greater than around  $3D$  downstream. In addition, the wake decay constant,  $k = 0.045$ , was tuned to obtain a best fit agreement with SOWFA in the far wake. The velocity deficit computed from the actuator disk model agrees with SOWFA, in general, at all locations downstream. It is important to note that the Park, DWM, and actuator disk model use an averaged actuator disk to represent the turbine. Tip vortices in the wake are not resolved and we cannot say anything definitive about their accuracy in the near wake. SOWFA implements an actuator line turbine model and is thought to give the closest representation of the near wake of the models presented.

Figure 4.2 compares power production, power variance, and average tower fore-aft bending moments on the downstream turbine for Park, DWM, and SOWFA model for the two-turbine setup (Figure 2.7). The actuator disk model has not been implemented for a two turbine setup. This will be implemented in future work. The results

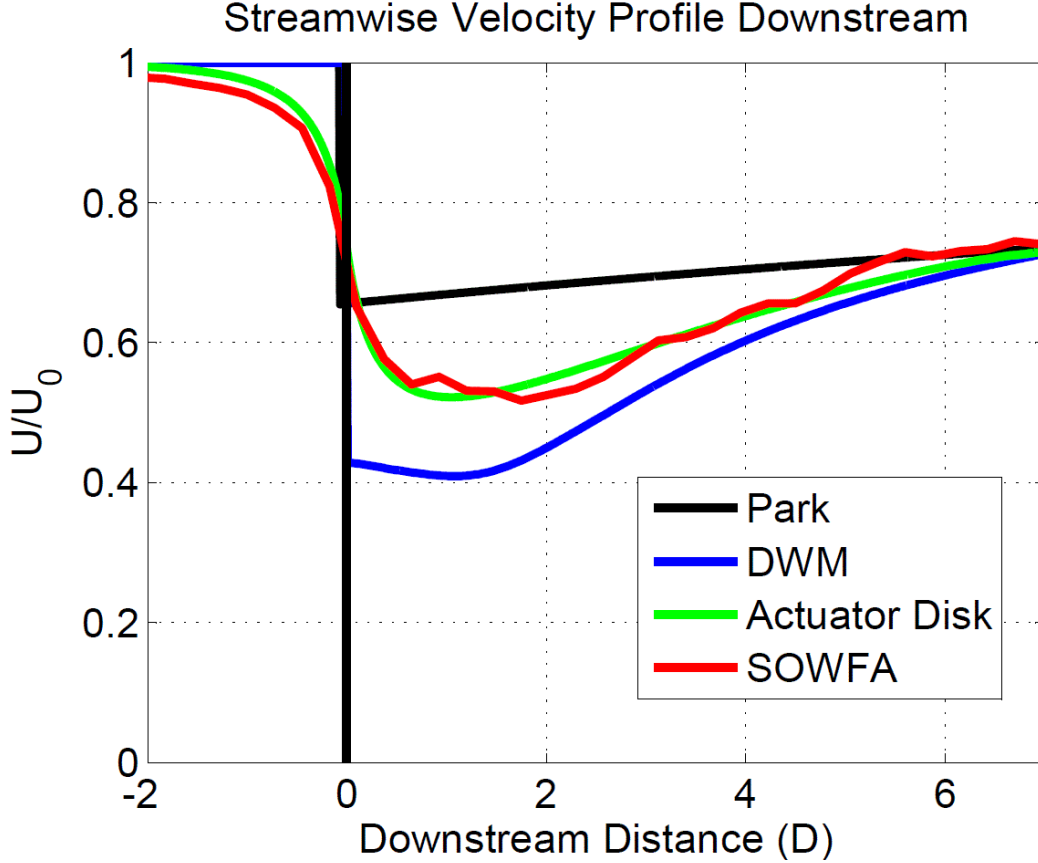


Figure 4.1: Comparison of Streamwise Velocity Downstream of the Turbine.

are presented for simulations with Turbine 2 placed with a downstream spacing of  $x = 2D$  to  $x = 7D$ . The average power results are consistent with the velocity profiles shown in Figure 4.1. The DWM model matches SOWFA best at turbine spacings of  $4D$  and greater. These results correspond to cases where the downstream turbine is in the far wake of the upstream turbine. The Park model follows the same trend but overestimates the power of the two-turbine array for turbine spacings less than  $5D$ .

The middle subplot of Figure 4.2 shows the power variance, and these results reflect the deviation in power over time. The Park model assumes steady flow and does not have a time component in the model. Thus the variance for this model is identically equal to zero for all turbine spacings. The DWM model shows an increase in power variance as the turbine spacing increases. This does not match the qualitative trend of the SOWFA results, which show that the power variance decreases as the turbine spacing increases. The limitations in the Park model can be seen in that it can only provide a total axial force on a turbine. SOWFA and the DWM model are coupled

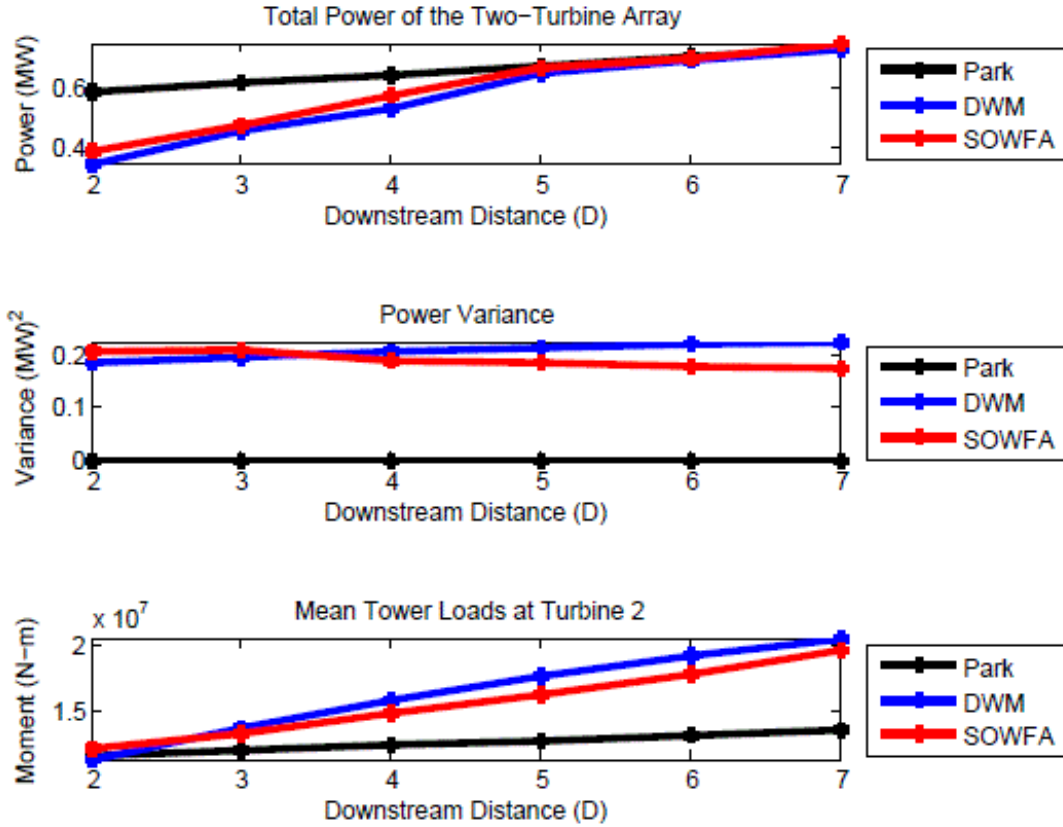


Figure 4.2: Power, Power Variance, and Tower Loads Computed for each model.

with FAST, hence they provide a more accurate description of the tower loads.

## 4.2 Open Loop Coordinated Control

This section provides results for two-turbine coordinated control on the Park and DWM models. The two-turbine coordinated control section formulated power maximization problems with realistic and simplified actuator disk models for a single turbine. In both cases, the maximum power from the two-turbine array is obtained by operating the rear turbine at its peak efficiency. Thus, the optimization reduces to a determination of the optimal derating for the lead turbine. The Park model uses an actuator disk model for the turbine with an induction factor control input. The Park model is relatively simple, hence the optimal induction factor for the lead turbine  $a_1$  can be determined numerically as previously demonstrated in [5].

Instead of optimizing the axial induction factor, the actuator disk model chooses a value of  $C_T^*$  for the front turbine that optimizes the power out of a two turbine array. The optimal induction factor for the actuator disk model can be computed from  $C_T^*$ . Results of axial induction control have not been shown for the actuator disk model as this model is still under construction for the two-turbine setup. The DWM model uses FAST to provide a more realistic turbine model and takes an input of blade pitch angle,  $\beta$ , and TSR,  $\lambda$ . The standard generator torque control law can be used to track the desired  $\lambda$ . After numerous open-loop runs at various  $(\beta, \lambda)$ , the optimal  $(\beta^*, \lambda^*)$  of the first turbine can be approximately determined. This  $(\beta^*, \lambda^*)$  can be mapped to a  $C_{P^*}$  value using a software package, WT\_Perf, developed at NREL [37]. The  $C_{P^*}$  can be related to the optimal induction factor using the actuator disk theory describe in the previous sections.  $C_P$  and  $C_T$ , as functions of the induction factor, are derived from simplistic models and are generally not realistic. However, they are close enough for axial induction factors to be compared across wake models. This approach only provides a suboptimal solution to the higher-fidelity power maximization problem. SOWFA also uses FAST to model the individual turbine dynamics, hence the approach described for the DWM model could also be used to generate control inputs for SOWFA.

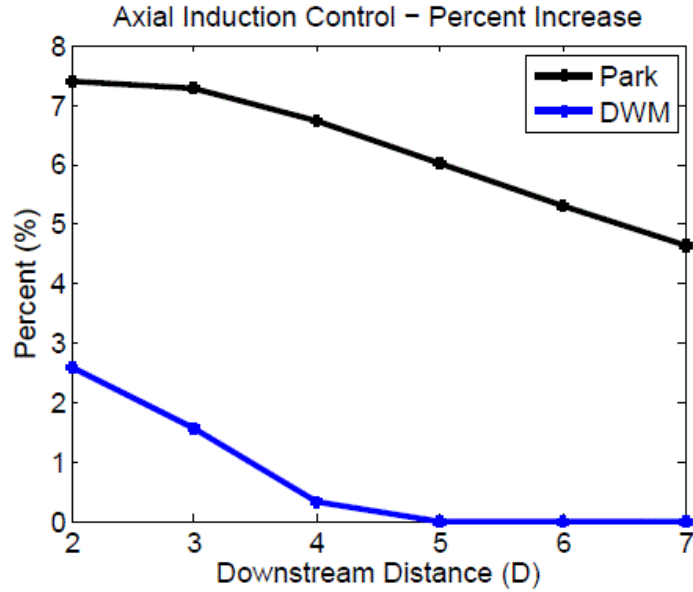


Figure 4.3: Percent Increase predicted using axial induction control.

Figure 4.3 shows the results of axial induction control with various wake models. The

Park model, with a tuned value of  $k$ , shows a decrease in power gained as the turbine spacing increases. The DWM model shows that there is an increase in power, but only for cases where the turbine spacing is less than 4 diameters. As the turbine spacing increases, there is more time for wake recovery. After a certain distance downstream of the turbine, the effects of axial induction control become less significant. Some simulations have been run in SOWFA at 4 and 7 diameter spacing. Although not shown, preliminary results in SOWFA show that there is very little power to be gained using axial induction control. This concept will need further investigation and validation.

### 4.3 Summary of Control Design and Analysis

Table 4.1 shows a summary of the models with some key components to consider when implementing wind farm control. The computation time represents the total time it took to run a 10-minute simulation. The Park, DWM, and actuator disk models were run on a desktop computer. SOWFA was run on 256 cores at the Minnesota Supercomputing Institute. The last column specifies the turbine model implemented in each wake model.

Model	Computation Time	Turbine Model
<b>Park Model</b>	5 seconds	One-dimensional
<b>DWM</b>	8 minutes	Actuator Disk
<b>Actuator Disk</b>	25 seconds	Actuator Disk
<b>SOWFA</b>	30 hours	Actuator Line

Table 4.1: Summary of Computation Time and Turbine Models for Wake Models.

The Park model is the fastest, simplest wake model and is suitable for feedback control. The induction factor is treated as the control input for a turbine in the Park model. Recall that the induction factor is related to the power coefficient through (5). By operating the first turbine at a suboptimal operating point, it may be possible to get more power out of the two-turbine array. Several studies have looked at this problem [2], [3], [4], [5], [6], [7], [13]. This model is only valid in the far wake, but gives an initial insight into how axial induction control might affect a two-turbine array.

The DWM model is a slower, but more complex model. It is harder to implement

dynamic feedback control because the DWM model calculates the flow field for each turbine over its entire simulation time. The model inputs, blade pitch angle and generator torque, can be used to control the power coefficient of the first turbine. The benefit of using this model is that it can use realistic turbine controllers at a low computational cost.

The actuator disk model can be used in dynamic feedback control. This model is also only valid in the far wake. The input to this model is the thrust coefficient. The thrust coefficient determines the loading on the actuator disk, which directly impacts the shape of the wake downstream. Figure 4.4 shows the difference between the actuator disk model and the Park model when computing the streamwise velocity component. The wake of the turbine looks very different showing the limitations of the Park model. The Park model assumes a constant velocity in the wake and the actuator disk shows the velocity varying across the width of the wake. This can have a significant impact on power and load calculations. Also, in terms of coordinated control, the operation of the front turbine influences the performance of the downstream turbine and since the wake development varies, the performance of the downstream turbine will be also be affected depending on the model used.

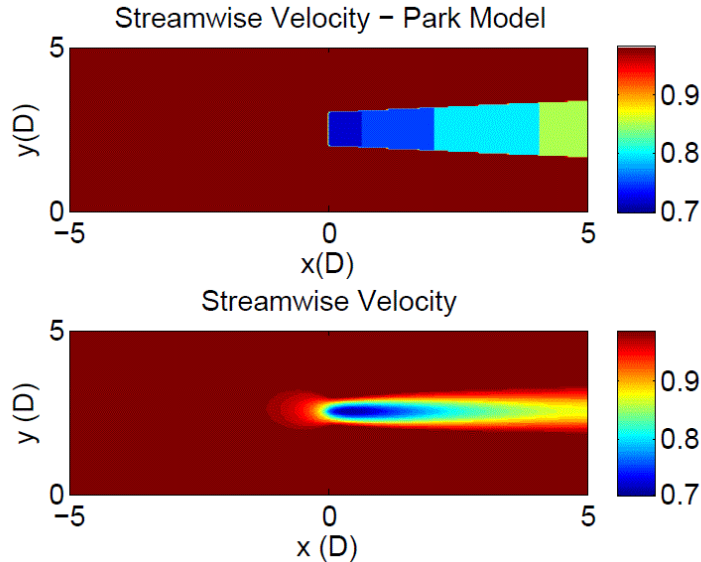


Figure 4.4: Streamwise Velocity of Park Model vs. Actuator Disk.

Lastly, SOWFA is a high-fidelity simulation tool. It can be used for feedback control. Like the DWM model, the inputs to the turbine model are blade pitch angle and

generator torque. Therefore, realistic turbine controllers can be tested with SOWFA. However, large amounts of computing resources would be necessary. A few studies have been done with open-loop control in SOWFA [35], [36]. Each simulation in SOWFA can help validate the lower-fidelity models and evaluate wind farm controllers, which can provide a better understanding of the wake interactions associated with particular wind farm setups.

# Chapter 5

## Model Validation

The University of Minnesota has a 2.5 MW Clipper Turbine at UMore Park in Rosemount, MN. The results from this experimental work is validated against the actuator disk model as it is the most dynamic model and the most likely candidate for control design and analysis in future work. Model validation is useful in exposing the limitations in these wake models and we can look to improve upon these models based on these findings. The overall goal of these experiments is to take measurements of the downstream velocity and compare it to the actuator disk model.

### 5.1 Experimental Setup

For these experiments, the Clipper Turbine in UMore Park (on the left in Figure 5.1) and the WINDCUBETM LiDAR (on the right in Figure 5.1) was used. The Clipper turbine has a diameter of 96m and a hub height of 80m. As stated previously, it produces 2.5 MW of power when operating at or above rated wind. The LiDAR was placed behind the turbine at various distances downstream of the turbine to measure the velocity in the wake of the turbine.

The LiDAR uses a pulsed laser that shoots out in four directions that are 90 degrees apart: north, south, east, and west. For the LiDAR used in these experiments, the beam is tilted at 27.83 degrees from vertical. The wind speed is computed by measuring the frequency shift of the backscattered light reflected off particles in the air at different heights. Using the measurement obtained from the lasers, it averages over the four beams to get a profile centered on the outlet window. Data is taken at



Figure 5.1: Clipper Wind Turbine located in UMore Park, Rosemount, MN (left). LIDAR used to measure wake profiles at various distances downstream (right)

a rate of 1 Hz.

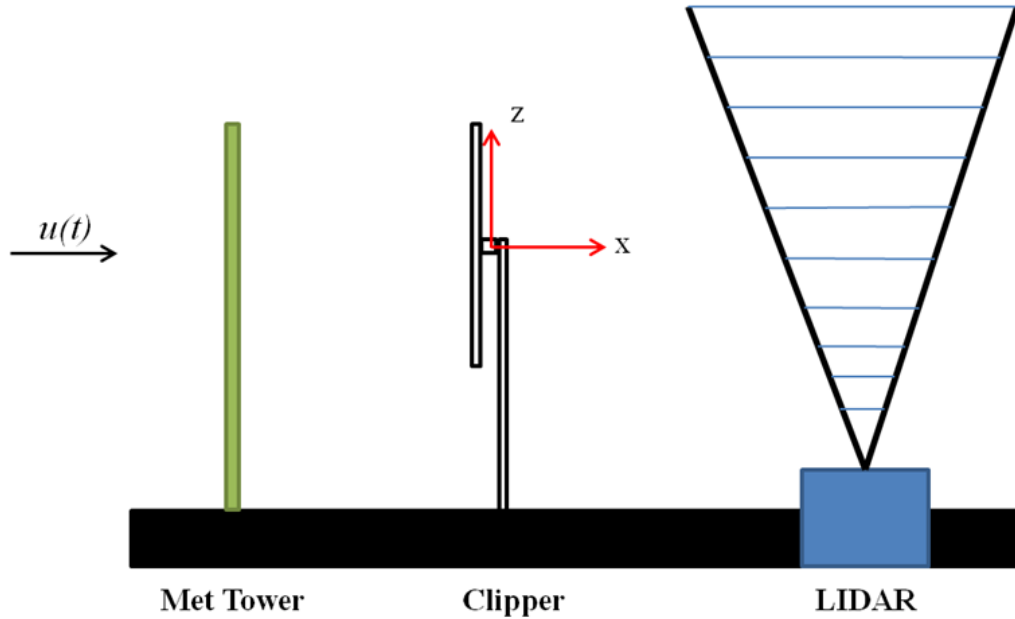


Figure 5.2: Wind Turbine/LIDAR Experimental Setup.

The experimental setup can be seen in Figure 5.2. On the particular day that the

experiments were run, the wind was coming out of the south. The meteorological (met) tower used to take measurements of wind speed at a fixed location is located directly south of the wind turbine. The met tower is located 1.67 Diameters up stream. This provided an accurate measurement of the inflow to the turbine. The LiDAR was placed at four different distances downstream: 1D, 1.5D, 2.5D and 3D. Measurements from the LiDAR were taken at 40m, 51m, 67m, 80m, 89m, 102m, 115m, 128m, 145m, and 160m above the ground. At each location, measurements are taken for about one hour.

## 5.2 Results

The LIDAR can provide some insight into the aerodynamics in the wake of a turbine. Since the LIDAR takes measurements at ten different vertical locations, the velocity profile at each distance downstream can be reconstructed and studied. Figure 5.3 shows the time-averaged wake profiles obtained at each downstream distance. The black line indicates the hub height of the turbine. At 1D downstream, the velocity profile exhibits a flow acceleration around the nacelle of the turbine giving the velocity profile an additional bump in the velocity profile. This behavior is expected because 1D is still in the near wake (see Figure 2.6) and this region is dominated by the geometry of the turbine and tip vortices. At 1.5D downstream, this acceleration around the nacelle diminishes and the velocity profile takes on a smoother shape, which is less dependent on the turbine geometry. At 2D and 3D downstream, the velocity profile becomes even smoother and starts to demonstrate self-similar behavior in which the shape of the profile is no longer dependent on the turbine geometry. Lastly, observing the wake profiles from 1.5D to 2.5D to 3D, the wake begins to recover as the velocity deficit in the observed wake is less and less.

Using measurements from the LiDAR at 80m, the velocity at hub height from the actuator disk model is compared to the time-averaged velocity from the LiDAR. The actuator disk model was fit to simulated data from SOWFA for a turbine with similar geometry under similar wind conditions (see Figure 4.1). This fitted model is what was compared to the velocity measured by the LiDAR. The input to this model is the thrust coefficient, which is dependent on the induction factor. On this day, the turbine had a power coefficient of 0.39. This translates to an induction factor of 0.128. Using the relationship between  $C_T$  and  $a$ , the input  $C_T$  is determined to be 0.4474. We do not expect to fit the data point at 1D. This is because 1D is in the near wake

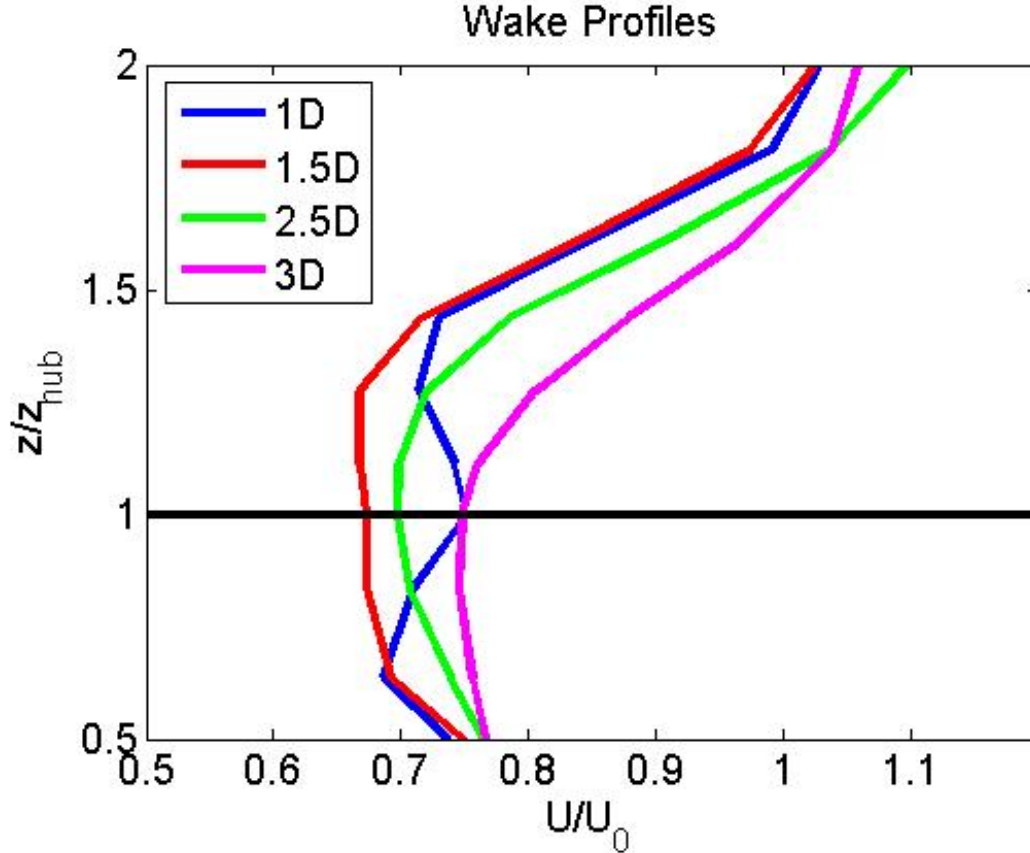


Figure 5.3: Wake Profiles gathered by LIDAR.

and has that acceleration in the velocity profile due to the turbine geometry. The actuator disk model does not include the turbine geometry. The turbine is modeled as a simple porous disk. As a result, that acceleration will not be seen in the actuator disk model. However, at 1.5D, the acceleration and the tip vortices start to die out and the actuator disk model can begin to capture the velocity at this distance. Similarly, at 2D, the actuator disk model lines up with the measurement taken at 2.5D.

Up until this point, the turbine operated in Region 2 where the turbine was maximizing power. However, at 3D the operating conditions of the turbine changed. The wind speed increased and the turbine entered Region 3 control which caused the turbine to keep a constant power and focus on minimizing loads. This action changes the nature of the wake. The turbine is trying to shed loads and power to keep power constant and not exceed the rated power. As a result, the wake deficit will be less than if the turbine was operating in Region 2.

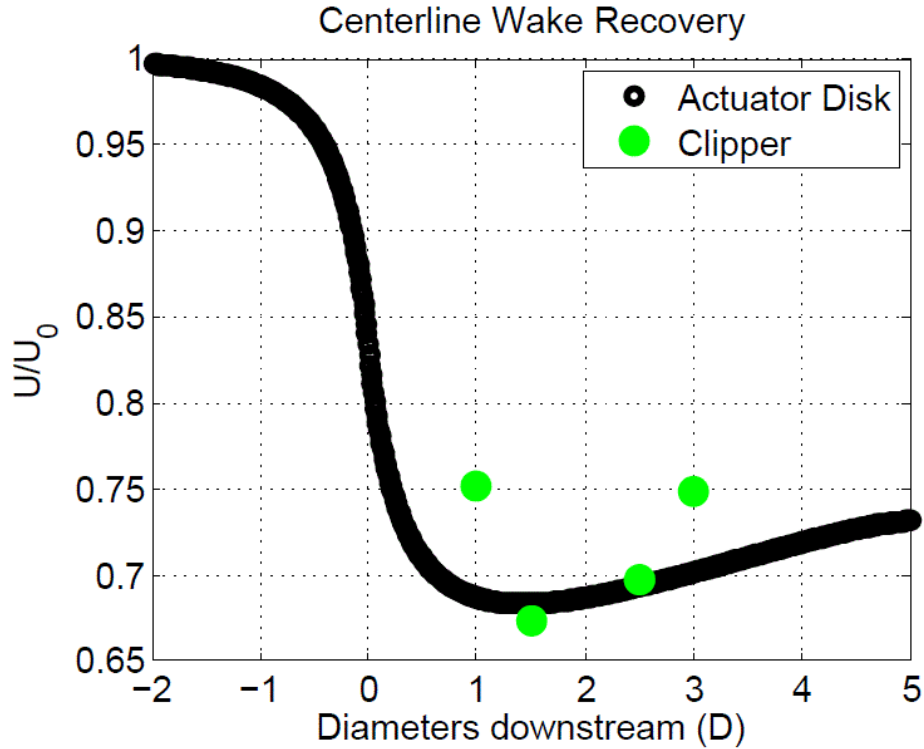


Figure 5.4: Actuator Disk with Comparisons of Downstream LIDAR Measurements.

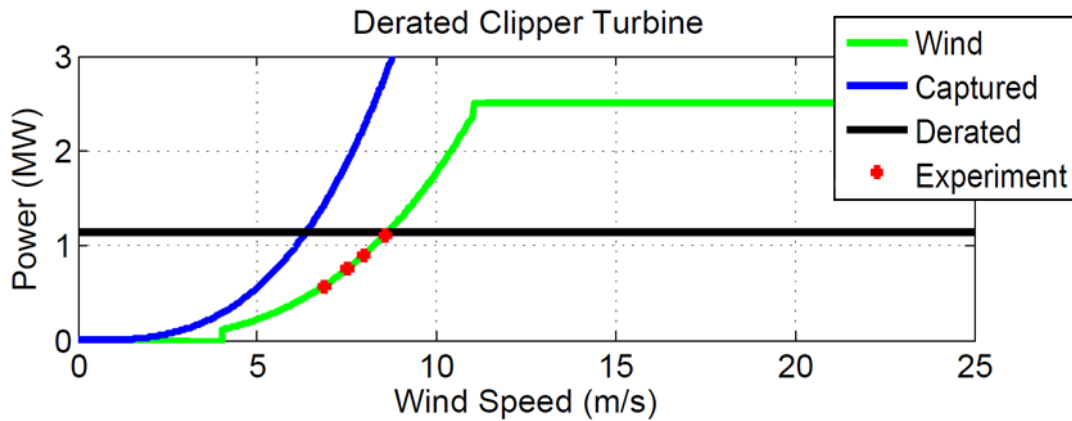


Figure 5.5: Operating Conditions during Experiments.

By changing the input parameter to this model, the actuator disk model can capture the point at 3D. However, it is important to note that wind farm control strategies, such as axial induction control, look to maximize power and would be implemented when the turbines are operating in Region 2.

Due to time and resource constraints, only four experiments were able to be run. This is not enough data to make any conclusions. However, preliminary results are promising.

# Chapter 6

## Conclusion

There is potential for optimizing wind farm performance by coordinating turbine controllers. Coordinated control design requires sufficiently high order models to retain the essential physics and provide an accurate depiction of the wake, while also minimizing the order model to enable feedback control with relatively low computational cost. Low-fidelity models can provide useful insight into wake interaction, but lack the complexity to provide realistic wind farm results. Medium fidelity models can capture many of the wake characteristics essential to wind farm control, specifically, power production and structural loads. However, medium fidelity models have made assumptions that simplify the aerodynamics in a wind farm and minimize computational cost. Both medium- and high-fidelity models are necessary for constructing an advanced controls framework that can be used to optimize turbine placement and control design in a wind farm.

Preliminary work has been done validating these wake models using experimental results from the Clipper turbine in UMore Park. Results show that medium fidelity models can capture the overall velocity trend in the wake. However, experimental time and resources were limited and more experimental data is necessary to draw concrete conclusions.

Future work will include evaluating these models using yaw control and investigating wake superposition in a wind farm with multiple rows and columns. This work will expand to include more turbines in various configurations to optimize power in a given area and number of turbines. Lastly, through the analysis of more experimental

results, it will be possible to reach conclusions regarding these wake models.

# Bibliography

- [1] Wisser, R., “Renewable Portfolio Standards in the United States - A Status Report with Data Through 2007,” LBNL-154E, Lawrence Berkeley National Laboratory, 2008.
- [2] Bitar, E. and Seiler, P., “Coordinated control of a wind turbine array for power maximization,” *American Control Conference*, 2013, pp. 2898–2904.
- [3] Gebraad, P. M. O., van Dam, F. C., and van Wingerden, J. W., “A model-free distributed approach for wind plant control,” *American Control Conference*, 2013, pp. 628–633.
- [4] Johnson, K. E. and Fritsch, G., “Assessment of Extremum Seeking Control for Wind Farm Energy Production,” *Wind Engineering*, Vol. 36, No. 6, 2012, pp. 701–716.
- [5] Johnson, K. E. and Thomas, N., “Wind farm control: Addressing the aerodynamic interaction among wind turbines,” *American Control Conference*, 2009, pp. 2104–2109.
- [6] Marden, J. R., Ruben, S., and Pao, L., “A model-free approach to wind farm control using game theoretic methods,” *IEEE Transactions on Control Systems Technology*, 2013, pp. 1207–1214.
- [7] Schepers, J. and Van der Pijl, S., “Improved modelling of wake aerodynamics and assessment of new farm control strategies,” *Journal of Physics: Conference Series*, Vol. 75 012039, 2007.
- [8] Machielse, L., Barth, S., Bot, E., Hendriks, H., and Schepers, G., “Evaluation of Heat and Flux Farm Control - Final Report,” ECN-E-07-105, Energy Research Centre of the Netherlands (ECN), 2007.

- [9] Jensen, N. O., “A note on wind generator interaction,” Tech. Rep. Risø-M-2411, Risø, 1983.
- [10] Ainslie, J. F., “Calculating the flowfield in the wake of wind turbines,” *Journal of Wind Engineering and Industrial Aerodynamics*, Vol. 27, No. 1, 1988, pp. 213–224.
- [11] Larsen, G. C., Madsen Aagaard, H., Bingöl, F., Mann, J., Ott, S., Sørensen, J. N., Okulov, V., Troldborg, N., Nielsen, N. M., Thomsen, K., et al., *Dynamic wake meandering modeling*, Risø National Laboratory, 2007.
- [12] Sørensen, J. N. and Myken, A., “Unsteady actuator disc model for horizontal axis wind turbines,” *Journal of Wind Engineering and Industrial Aerodynamics*, Vol. 39, No. 1, 1992, pp. 139–149.
- [13] Torres, P., van Wingerden, J.-W., and Verhaegen, M., “Modeling of the flow in wind farms for total power optimization,” *Int. Conference on Control and Automation (ICCA)*, 2011, pp. 963–968.
- [14] Mikkelsen, R., *Actuator disc methods applied to wind turbines*, Ph.D. thesis, Technical University of Denmark, 2003.
- [15] Yang, X. and Sotiropoulos, F., “On the predictive capabilities of LES-actuator disk model in simulating turbulence past wind turbines and farms,” *American Control Conference*, 2013, pp. 2878–2883.
- [16] Churchfield, M. and Lee, S., “NWTC design codes-SOWFA,” <http://wind.nrel.gov/designcodes/simulators/SOWFA>, 2012.
- [17] Gebraad, P., Teeuwisse, F., van Wingerden, J., Fleming, P., Ruben, S., Marden, J., and Pao, L., “A Data-Driven Model for Wind Plant Power Optimization by Yaw Control,” *Power [W]*, Vol. 1, pp. 1–5.
- [18] Johnson, K. E., Pao, L. Y., Balas, M. J., and Fingersh, L. J., “Control of variable-speed wind turbines: standard and adaptive techniques for maximizing energy capture,” *Control Systems, IEEE*, Vol. 26, No. 3, 2006, pp. 70–81.
- [19] Pao, L. Y. and Johnson, K. E., “Control of wind turbines,” *Control Systems, IEEE*, Vol. 31, No. 2, 2011, pp. 44–62.

- [20] Burton, T., Jenkins, N., Sharpe, D., and Bossanyi, E., *Wind energy handbook*, John Wiley & Sons, 2011.
- [21] Jonkman, J., “NWTC Design Codes - FAST,” <http://wind.nrel.gov/designcodes/simulators/fast>, 2010.
- [22] Van Kuik, G. A., “The Lanchester–Betz–Joukowsky limit,” *Wind Energy*, Vol. 10, No. 3, 2007, pp. 289–291.
- [23] Sanderse, B., “Aerodynamics of wind turbine wakes,” *Energy Research Center of the Netherlands (ECN), ECN-E-09-016, Petten, The Netherlands, Tech. Rep*, 2009.
- [24] Katic, I., Højstrup, J., and Jensen, N., “A simple model for cluster efficiency,” *EWECC*, 1986, pp. 407–410.
- [25] Sørensen, T., Thøgersen, M. L., Nielsen, P., and Jernesvej, N., “Adapting and calibration of existing wake models to meet the conditions inside offshore wind farms,” *EMD International A/S. Aalborg*, 2008.
- [26] González-Longatt, F., Wall, P., and Terzija, V., “Wake effect in wind farm performance: Steady-state and dynamic behavior,” *Renewable Energy*, Vol. 39, No. 1, 2012, pp. 329–338.
- [27] Hao, Y., Lackner, M., Keck, R.-E., Lee, S., Churchfield, M., and Moriarty, P., “Implementing the Dynamic Wake Meandering Model in the NWTC Design Codes,” *AIAA*, 2013.
- [28] Sørensen, J. N. and Kock, C. W., “A model for unsteady rotor aerodynamics,” *Journal of wind engineering and industrial aerodynamics*, Vol. 58, No. 3, 1995, pp. 259–275.
- [29] Zikanov, O., *Essential computational fluid dynamics*, John Wiley & Sons, 2010.
- [30] Schlichting, H. and Gersten, K., *Boundary-layer theory*, Springer, 2000.
- [31] Fleming, P., Gebraad, P., Churchfield, M., Lee, S., Johnson, K., Michalakes, J., van Wingerden, J.-W., and Moriarty, P., “SOWFA + Super Controller User’s Manual,” Tech. rep., National Renewable Energy Laboratory (NREL), Golden, CO, 2013.

- [32] Fleming, P., Gebraad, P., van Wingerden, J.-W., Lee, S., Churchfield, M., Scholbrock, A., Michalakes, J., Johnson, K., and Moriarty, P., “The SOWFA Super-Controller: A High-Fidelity Tool for Evaluating Wind Plant Control Approaches,” Tech. rep., National Renewable Energy Laboratory (NREL), Golden, CO, 2013, Proc. of the EWEA 2013.
- [33] Churchfield, M. J., Lee, S., Michalakes, J., and Moriarty, P. J., “A numerical study of the effects of atmospheric and wake turbulence on wind turbine dynamics,” *Journal of Turbulence*, , No. 13, 2012, pp. 1–32.
- [34] Churchfield, M. J., Lee, S., Moriarty, P. J., Martinez, L. A., Leonardi, S., Vijayakumar, G., and Brasseur, J. G., “A large-eddy simulation of wind-plant aerodynamics,” *Proc. of 50th AIAA Aerospace Sciences Meeting*, 2012, pp. 9–12.
- [35] Fleming, P., Gebraad, P., Churchfield, M., Lee, S., Johnson, K., Michalakes, J., van Wingerden, J.-W., and Moriarty, P., “Evaluating techniques for redirecting turbine wakes using SOWFA,” 2013, Proc. of ICOWES.
- [36] Fleming, P., Gebraad, P., Churchfield, M., Lee, S., Johnson, K., Michalakes, J., van Wingerden, J.-W., and Moriarty, P., “High-fidelity simulation comparison of wake mitigation control strategies for a two-turbine case,” 2013, Proc. of ICOWES.
- [37] Platt, A., “NWTC Design Codes WT-Perf,” <http://wind.nrel.gov/designcodes/simulators/wtperf/>, 2012.